A Fast Algorithm for Altimeter Waveform Retracing with Applications to the Geosat Altimeter

Ernesto Rodríguez and Jan M. Martin
Jet Propulsion laboratory
California Institute of Technology
4800 Oak Grove Dr., Pasadena, CA 91109

Abstract

The real time processing of ocean altimeter waveform data to obtain higher accuracy ocean surface height fields has long been thought desirable, but not feasible due to the computational cost of existing waveform processing algorithms. The desirability of such an algorithm is emphasized hy the improvements in orbital predictions and geoid models, which make tile detection of several centimeter level signals using the Topex/Posidon mission feasible. In this paper, we present a new technique for faster than real time estimation of height from altimeter waveforms using modest computer resources, The algorithm is tested theoretically using Monte Carlo simulations and practically using waveform data from the Geosat altimeter mission. We also examine the source of errors for the Geosat heights, and study the possibility of making empirical polynomial corrections using waveform fitting. We pay special attention to the length of time needed to estimate accurate corrections as well as the functional form such corrections should take. The importance of the non-Gaussian nature of the sea surface in producing height biases which me correlated with sea state is also examined.

1. Introduction

Satellite altimeters have demonstrated the capability of mapping ocean mesoscale variability and have shown potential in determining basin scale circulation, The TOPEX mission [Zieger et al., 1991] features precision in the orbit determination and the correction for geophysical propagation effects sufficient to determine global scale circulation. As the errors due to the orbit and propagation effects are reduced, it becomes increasingly desirable to also reduce the errors due to the height estimation algorithm. These errors include both short wavelength random noise, and, more importantly, potential long wavelength errors due to significant wave height (SWH) biases and altimeter misprinting, or the presence of unmodeled ocean surface effects, such as the surface skewness [Rodríguez, 1988].

In addition to the onboard height estimates, satellite altimeters also return the radar signs], or waveform. This waveform contains information about the surface height, SWH, backscatter cross section (which may be related to wind speed), altimeter attitude, and surface skewness. The onboard height estimation algorithm is of necessity rather crude [Chelton

et al. 19,S{)] and an improved estimate of the various parameters can he obtained by using more optimal algorithms. The most commonly used algorithm is the least square fitting of the altimeter return [Hayne and Hancock, 1991]. The implementation of this algorithm suffers from the disadvantage that the fitting function cannot he expressed analytically and numerical derivatives had to be computed. This makes the algorithm unsuitable for real time processing of the waveform data. In order' to obtain an analytic fitting function, the deconvolution method [I, ipa and Barrick, 19S1], [Rodríguez,1988], [Rodriguez and Chapman,1989] was introduced and shown to give real time unbiased estimates for the height. However, neither of these algorithms was optimal, in a statistical sense. A maximum likelihood algorithm was derived in [Rodríguez,1988] and [Srokosz, 1988]. This algorithm has the potential of greater accuracy than the previous two algorithms, but again suffers from the disadvantage that it is numerically slow, due to the fact that the fitting function is not analytic. An alternate approach to reprocessing the data has been presented by Brenner et al. [1993], a parametrization of the return waveform which is not hased on the convolution model of Brown [1977]. The method proposed in that paper was shown to improve the oceanographic height signal, but also suffered from being computationally slow, and was not based on the physical scattering theory, which allows, in principle, the recovery of ocean surface parameters. In this paper, we solve the problem of how to make the fitting function analytic, thus allowing for faster than real time processing of altimeter waveforms resulting in very high accuracy determination of sea state parameters.

The derivation of the fitting algorithm and its performance for the TOPEX and Geosat altimeters are discussed in the first two sections of this paper. In the third section, we apply the algorithm to Geosat data. We show how the nominal Geosat point target response can be shown to he in error, and discuss the estimation of the true point target response from the data. Finally, we use our algorithm to derive corrections based on SWH and attitude and compare against the work of Hayne and Hancock [1991].

2. The Fitting Algorithm

The maximum likelihood function, including the effects of bin-to-bin and pulse-to-pulse

signal correlations, was derived in [Rodríguez,1988]. Its logarithm is given by

$$\ln f_{\mathrm{ML}}(a_j) = \frac{n}{2}(\ln 2\pi) + \frac{1}{2}\sum_i \left[\ln(e_i(a_j) + \frac{v_i^2(a_j)}{e_i(a_j)}\right] \tag{1}$$

where n is the number of data samples, the a_j represent the waveform parameters, the e_i are the eigenvalues of the correlation matrix for the return waveform

$$C_{ij} \equiv S^{\mathrm{T}} DS \equiv \langle x_i x_j \rangle \tag{2}$$

$$x_i = p_i - P_i(a_j) - N \tag{3}$$

where p_i is the return power in the ith bin, $P_i(a_j)$ is the mean expected signal power given the fitting parameters, N is the mean expected noise power, D is a diagonal matrix whose ith element is e_i, and S is an orthogonal transformation. Finally, the vector v_i is defined by

$$\vec{v} = S\vec{x} \tag{4}$$

In general, the correlation matrix is not diagonal: the waveform samples are correlated with each other due to the finite sidelobes of the altimeter point target response [Berger, 1'072], [Rodriguez and Martin, 1992]. This makes the task of estimation cumbersome since at each step of the estimation process the correlation matrix must be calculated and diagonalized. However, in theoretics] and experimental studies [Rodriguez and Martin, 1992] we have shown that the correlations are small, and we will ignore them henceforth. (The effect of ignoring these correlations will be discussed below). In addition, we will also ignore the factor $\sum_i \ln(e_i(a_j))$ as we have found that this factor, since it is not data driven, affects the minimum of the maximum likelihood function very little. Making these assumptions our sub-maximum likelihood estimator is given by

$$\ln f_{\mathrm{SML}} = \sum_i \left(\frac{p_i - P_i - N}{P_i/n_i + N/n}\right)^2 \tag{5}$$

where some constant factors have been neglected. In the previous expression, n_i is the number of independent signal samples. Due to the effects of pulse-to-pulse correlation, the number of independent signal samples need not be the same as the number of waveforms

[Berger, 1972], [Lipa and Barrick, 1981], [Rodríguez and Martin, 1992]. The value of n_i again depends on the waveform parameters and cannot be coded efficiently enough for real time processing. For the sake of computational efficiency, we set $n_i = n$. This will only be noticeable in the early part of the leading edge and for low SWH, when pulse-to-pulse correlation effects may be noticeable. If these assumptions are made, the sub-maximum likelihood estimator is equivalent to the "maximum likelihood estimator" derived in [Srokosz, 19ss], when all the correlation effects were neglected. The problem is reduced to weighted least squares estimation, where the the weighting function is the mean waveform. Rather than calculating this quantity iteratively, we use the fact that over short time spans the ocean parameters, and hence the mean waveform, change very little. Thus a good estimate of the mean waveform to be employed in weighting the residues can be obtained by simply averaging the data:

$$\sigma_i \equiv P_i + N \approx \frac{1}{m} \sum_{j=1}^{m} p_i^{(j)} \tag{6}$$

where the sum extends over the number of waveforms averaged. For Geosat, for instance, after averaging one second's worth of waveforms, one obtains the waveform to approximately 3% accuracy. For the TOPEX altimeter, which has a higher pulse repetition frequency (PRF), one second averaging yields the mean waveform to approximately 1.670 accuracy.

Finally, it is useful to reduce the number of estimated parameters in order to increase the stability of the solution. The return waveform is fully characterized by the following set of parameters: the surface standard deviation σ, the tracker height offset δh, the skewness of the specular point distribution λ, the off-n adir angle ξ, the surface radar cross section σ_0, and the thermal noise level, N. The thermal noise level does not change over short periods of time. Since it is a Gaussian process with constant mean, and since the beginning of each waveform record starts with a section where no signal is present, we estimate the thermal noise level separately as

$$\hat{N} = \frac{1}{km} \sum_{j=1}^{m} \sum_{i=1}^{k} p_i^{(j)} \tag{7}$$

where the first sum extends over the different waveforms, and the second sum extends over

the waveform samples in the thermal noise region of the waveform. As is well known [Sorenson, 1980], this is the maximum likelihood estimator for the thermal noise. In our processing, this constant value is subtracted from all the waveforms used to form its estimate.

After making the previous assumptions, the waveform parameters can be estimated by minimizing $\ln f_{SML}$. This function is highly nonlinear in the waveform parameters, which makes the task of minimization non-trivial. We make use of the fact that the waveform will be reprocessed on the ground, when the nominal altimeter algorithms already give good estimates for all of the waveform parameters, and linearize about an initial set of estimates, a_j = a:");- δa_j. Minimization of the sub-likelihood function is then equivalent to solving the following linear least squares problem

$$\sum \alpha_{ij} \delta a_j = \beta_i \tag{8}$$

$$\alpha_{ij} = \sum_k \frac{\partial P_k}{\partial a_i} \frac{\partial P_k}{\partial a_j} \frac{1}{\sigma_k^2} \tag{9}$$

$$\beta_i = \sum_j \frac{p_j - P_j}{\sigma_j^2} \frac{\partial P_j}{\partial a_i} \tag{10}$$

Even after the previous approximations have been made, the problem is still computationally intensive, due to the fact that the mean altimeter waveform and the derivatives of the waveform are not analytic functions, in general. The mean return waveform can be expressed as the convolution of three terms: the surface impulse response [Brown, 1977] [Rodríguez, 1988], the specular point probability density function, and the instrument point target response (ptr), $\chi(t)$. An analytic expression exists for the mean return waveform only when $\chi(t)$ is a Gaussian. Unfortunately, for most altimeters, including Seasat, Geosat and TOPEX, the point target response is a non-analytic function which resembles a sine function squared ancl is obtained by measurement during the altimeter calibration.

in order to solve this problem, and in the spirit of the wavelet transform, we expand $\chi(t)$ as a sum of Gaussians of different amplitudes, means and standard deviations

$$\chi(t) = \sum_i c_i \exp\left[-\frac{(t - t_i)^2}{2s_i^2}\right] \tag{11}$$

Our fitting method for tile c_i's, s_i's, and t_i's proceeds iteratively. First, we take the square root of the altimeter calibrated point target response and alternate the signs of the peaks to obtain the point target response in the voltage domain, which is now Nyquist sampled. We then Nyquist interpolate tile point target response to achieve oversampling. We perform a sequential least square fit of ii Gaussian function for each of the interpolated ptr peaks, starting with the largest and progressing to the smallest, The residuals of this initial fit are then fit again with another set of Gaussians, and this procedure is continued until the desired accuracy is obtained. Figure 1 presents a comparison of the ideal point target reponse and Gaussian fits. As can be seen, the fit is excellent and further accuracy can be obtained by additional iterations, but this would be unwarranted given the accuracy of the calibration point target response, which is approximately 170 [Hayne, private communication]. Using this approximation, the derivatives of the mean waveform with respect to the waveform parameters are easily calculated, The results are presented in Appendix A.

3. Theoretical Performance

To assess the accuracy of the previous algorithm, we performed a Monte Carlo simulation of the fitting procedure. Although the final fitting is linear, and one can formally estimate the fitting errors, this estimate does not take into account various possible additional sources of error. We mention possible breakdowns in the linearization assumption, and the neglect of pulse-to-pulse correlation and quantization effects.

Our simulation procedure is described fully in [Rodriguez and Chapman, 1989]. Here, we present a brief description of the main steps. The Geosat telemetry waveform consists of tile average of 100 pulses, and the pulse repetition frequency (prf) is approximately 1 KHz. Topex will be transmitting waveforms for Ku-band (14.4 (; Hz) and C-band (5.6 GHz). The Ku-band prf is approximately 4 KHz, while the C-band prf is approximately 1 KHz. Each Ku-band waveform will consist of the average of 456 pulses, while each C-band waveform will be the average of 110 pulses.

To simulate the estimation process, we generated mean waveforms and added Gaussian noise to each waveform. The variance of the noise was determined by the number of pulses,

the signal-to-noise ratio (snr), and the pulse-to-pulse correlation properties of the waveform. To take this last factor into account, we calculated the decorrelation time by using the van Cittert-Zernike theorem [V Valsh, 19 82], and, from this, the number of independent pulse samples. This number differed from the number of pulses only in the leading edge region and only for the higher prf. The variance of the Gaussian noise was set equal to the mean waveform value divided by the number of independent samples. The waveform was then quantized to 8-bits, as in Geosat or Topex, by an adaptive quantizer which took into account the largest waveform value.

Simulations were performed for a variety of swh, skewness, and attitude values. The noisy estimated parameters, with the exception of the skewness, were passed through a smoothing filter and the result of this filtering was used for the linearization of the estimation process. The time constant of the filter was set to three seconds, which is equivalent to the filtering used by existing altimeters.

Results of these Monte Carlo simulations for the Topex altimeter are presented in Figure i! and contrasted against the requirements set for the Topex mission. The results for Geosat are compared to the actual performance in the next section, As can be seen from Figure 2, the fitting technique proposed here more than meets the performance requirements. We note that Figure 2c shows that the accurate estimation of the skewness parameter is feasible given a moderate amount of averaging.

4. Retracing of Geosat Waveforms

In order to assess the performance of this waveform fitting algorithm under more realistic conditions than the Monte Carlo tests described in the previous secion, we processed two weeks of waveform data from the later part part of the Geosat Exact Repeat Mission (ERM): February 29, 1988 to March 13, 1988. The measured Geosat point target response [Geosat ICD] was fit by a set of Gaussian functions with a cutoff amplitude of 10^{-4} which produced a representation with errors of absolute magnitude less than than 0.004 when the peak of the PTR is normalized to unity. Both weighted and unweighted fitting procedures were tested *011* this Geosat data set.

The results of this first trial on real data showed reasonable agreement with Geophysical Data Records (GDR) values of SWH, but the height corrections were not in very good agreement with the GDR values. More significantly, the skewness results were completely unphysical- much too large in magnitude and negative in sign, especially for small values of SWH. The source of the discrepancy is indicated by the dashed curves in Figure 3a, which shows the difference between the fitted theoretical waveform using the Geosat PTR and the measured waveform normalized by the measured waveform, averaged over all waveforms corresponding to GDR SWH between 1.0 and 1.5 m in one day of data (2/29/88). This selection reduced the masking effects of larger SWH sea states on the waveform. The relatively large (20%) negative excursion in the residual curve corresponding to the leading edge of the average waveform shown above shows that the theoretical or fitted waveform is consistently too large in this region, which suggests that the theoretical PTR has sidelobes which are too large and explains the observed large negative values of the estimated skewness as an attempt by the fitting procedure to compensate for this error. The dashed curve in Figure 3b shows that this result is not a product of the fitting procedure, as the weighted residues here are the differences between the theoretical waveform defined by the Geosat GDR values of SWH, ξ, and Δh, with $\lambda = 0$. The same curve shape is evident. We conclude that the calibration procedure used to obtain the point target response was contaminated resulting in significant systematic errors.

In the absence of better measurement of the instrument PTR, we attempted to find a better fitting using a simple parametrized model. The model consisted of the theoretical PTR, a sinc^2 function, modified by a symmetrical linear weighting function. Our best estimate for the Geosat PTR thus is

$$\mathrm{PTR}(\tau) = \left(\frac{\sin(\pi B\tau)}{\pi B\tau}\cdot\frac{(1 + |\tau|/T)}{}\right)^2 (1 - \alpha|\tau|)$$

where B is the chirp bandwidth, T is the chirp duration, and $\alpha = 0.002$ is the weighting constant. Both the original Geosat PTR and the new PTR are plotted in Figure 4 along with the difference, which shows that the main peak is narrower and the first sidelobe is significantly decreased in the new PTR, as required. This choice of PTR produces the solid

weighted residual curves in Figure 3. Note that using the Geosat parameters leaves a +10% error in the leading edge which is removed by the fitting process (Figure 3a).

The random-seeming fluctuations at the sub-1% level are for the most part consistent from data set to data set, and are tllcr{'fore due to slight errors in the multiplicative scaling factors used to correct for the filter gains in the altimeter correlator[Geosat ICD]. Six of the multipliers initially produced errors greater than 1% and they were corrected to bring error level back to the 1 % level - complete correction of the multiplier errors was not attempted due the presence of residual PTR-induced errors already at the 1% level. This limited multiplier correction is also reflected in the solid curves of Figure 3. Similar processing was also run on two other days in the tivo-week data period, with similar (to $\pm 0.2\%$) results.

Using this corrected 1''1'}{, we retracked the full two-week Geosat data set using the GDR values for SWH, Δh, and ξ, and $\lambda = 0.0$ as initial values for both weighted and unweighed fitting algorithms. As a first check on the algorithm performance, we calculated the height correction standard deviation over each 10 sec averaging interval and plotted it against the mean SWH over the same interval in a scatter plot. These results are shown in Figure 5 for both weighted and unweighted algorithms, along with solid lines showing the expected dependence obtained from the Monte Carlo simulations. Although the scatter is large, as expected, the overall levels and slopes are consistent, showing slightly decreased level and dependency on SW} I using the weighted algorithm. This suggests that the Monte Carlo estimates described in the previous section will be useful guides to the expected performance of the retracing algorithm.

Comparison between the Geosat GDR estimates for SWH, ξ^2, and δh (dhsa) and the results of the retracing algorithm are shown in Figure 6a, b, and c, respectively. Weighted and unweighted fits produced the same results, so only the unweighed fits are shown. Each graph represents the result of 35,.500 waveform fits, with the distribution of the results shown at the top, and the 1-σ standard deviations given by the error bars. Figure 6a shows the SWH comparison: the retracked SWH is higher than the GDR value by a nearly constant offset of 22 cm. The lower GDR value is consistent with the positive peak in the

residual curve in Figure 3b. The comparison of squared-attitude ξ^2 is shown in Figure 6b, where the retracked values are generally less than the GDR values by 0.08 degrees^2 over the range 0.1 to 1.3 degrees^2 which contains most of the data. At higher attitudes of 1.2 to 1.7 deg^2 the retracked values increase to levels significantly greater than tile GDR values (+0.4 at 1.7 deg^2), but these conditions are too rare to significantly affect the average weighted residuals shown in Figure 3. The higher GDR values are also consistent with the small but clearly visible slope in the tail of the residual curves in Figure lb, which is again removed by tile fitting process. Finally, GDR and retracked height corrections δh are plotted in Figure 6c. The average retracked height correction is 1.01 cm greater than the GDR data, but the retracked points clearly show by their shallower slope that the retracking algorithm calculates less height correction than the standard Geosat algorithm over the whole range shown (except for a small offset around O). over the interval -10cm to +5cm which contains most of the data, the retracked corrections range from -8cm to +2cm. The large variances in these data are due only partly to noise- since δh bias has been shown to depend on SWH and ξ^2 as well as δh, variation of these quantities will increase the variances shown in each bin of Figure 6c. We will investigate these dependencies in more detail in the next section.

5. Polynomial Corrections to Geosat Data

For Geosat, there are two likely sources for height errors for Geosat: errors due to attit ude; and, errors due to the skewn ess bias. The Geosat satellite was gravity gradient stabilized which caused it to have relatively large oscillations in attitude relative to the ocean geoid: attitudes greater than one degree were not uncommon. The altimeter tracker suffers biases due to off-nadir pointing which must subsequently be corrected (luring the ground processing. For Geosat, the spacecraft attitude was not known to a good enough accuracy to make these corrections and corrections were made based on the altimeter waveform trailing edge. During this processing, errors may be introduced if the relationship between attitude and waveform are not modeled correctly. The height correction due to attitude errors is modeled roughly as being linearly dependent on the product of the SWH and the square of the attitude. If the slope is this relationship is in error, one would expect to see a linear

trend in the residual height error proportional to this product.

A second unmodeled error source is the skewness bias [Rodríguez, 1989]: the presence of ocean surface skewness introduces a bias which is proportional to the product of skewness times the SWH. Figure 7 presents a histogram of the skewness estimated by the algorithm for days 60-73 of 1988. The mean skewness value is about 0.15 and the bulk of the observed skewness values lie between 0 an 0.3. This is consistent with theoretical predictions and the scant observation made of this quantity [Srokosz and Longuet-Higgins, 1986]. A small number of negative skewness values were observed, but we believe that these arc clue to estimation noise, rather than to actual negative values. A further discussion of the characteristics of the observed skewness for both Geosat and Topex will be presented elsewhere. In this paper, we limit ourselves to study its effect on the height bias.

'1'0 test the hypothesis for the sources of the height error, we present in Figure 8a the residual height error from the waveform retracing binned as a function of the two parameters mentioned above for days 60-73 of 1988. This data shows a clear linear trend as a function of these two parameters. In Figure 8b we present the residual errors after a linear function is removed from the results presented in Figure 8a. The residual error after this linear function is removed is below half a centimeter over most of the data range giving a clear indication that these two sources of error are sufficient to account for the systematic errors in the Geosat tracker.

Since the ocean surface skewness is not routinely available for making height corrections, a separate approach has been taken to obtain height corrections. Hayne et al. [1991] have advocated the idea of using retracked waveform results to obtain polynomial corrections in terms of parameters available as part of the available Geophysical Data Record. A possible, though not unique, choice of parameters is the SWH and the estimated attitude. The idea behind this method is that these parameters are correlated to the true error sources and applying an empirical correction based on these parameters may remove the bulk of the errors. Hayne et al. [1991] presented an example of these correction polynomials based on a limited set of Geosat data.

Since the corrections are empirically derived, one must average over a large data set to sample the parameter space sufficiently and to obtain a statistically meaningful estimate for the polynomial coefficients. The necessary length of time was not addressed by Hayne et al. [1991]. In this paper, we study this requirement by averaging the residual height error as a function of SWH and attitude for different integration times. Figures 9a and 9b present contour plots of the residual height error for two different averaging periods of one week. Although there are similar trends in the two sets of contours, there are also marked differences. This is especially true where not much data exists, such as at high attitudes or high values of SWH. However, even at low values of SWH differences between the two data sets are apparent. Figure 9c presents a similar plot, but in this case the averaging time is two weeks. As can be seen, for this case the contours are smoother and better behaved, even for high attitudes. We conclude that at least this amount of averaging is required in order to obtain stable estimates for the correction coefficients.

Another question left open by Hayne et al. is what the degree of the fitting polynomial should be. To study this question, we fit second and third order polynomials to the error surface presented in Figure 9c. To take into account the fact that different regions of parameter space are visited with different frequency, each data point in the fit represented the average over a bin in parameter space and was weighted by the standard error (i.e. the sample standard deviation divided by the square root of the number of points in the bin) when performing the fit, The resulting fits, together with the residual error surfaces, are presented in Figure 10. We observe from these results that, over the bulk of the data, a cubic fit does not offer a significant improvement over a quadratic fit. About the edges of parameter space, the cubic does offer some improvement. However, at the very edge of the parameter space (high attitude) the cubic errors can be greater than those of the quadratic fit. This is to be expected since it is widely known that polynomial fits can be quite inaccurate when extended outside the part of parameter space most heavily weighted in the fitting. We conclude that for Geosat, a quadratic fitting function is more robust and probably sufficient to correct for the bulk of the mean height error. Nevertheless,

since skewness and SWH are independent parameters, one cannot correct completely for the Skewness bias by making a correction based on SWH done: one will correct for the global mean of skewness bias, but the height residuals will still show a linear trend with the product of skewness and SWH.

6. Conclusions

It has long been recognized in the altimetric community that it would be desirable to reprocess altimeter waveform data in order to obtain improved altimeter performance [Brenner et al., 1993]. The major obstacle towards this goal has been the amount of processing time required by processing algorithms: the traditional belief has been that waveform processing could only be done at a rate much slower than real time, thus making it unfeasible for operational use. In this paper we introduce a method which overcomes these problems and allows for faster than real time processing of altimeter data using modest computer resources. We have shown that this method produces accurate altimeter heights and SWH's, as well as estimates of the skewness of the return waveform. We presented the results of applying this algorithm to Geosat data demonstrated the noise performance of the algorithm consistent with theoretical estimates. We also showed that the Geosat heights available in the Geophysical Data Record suffer from biases, and ascribed these biases to attitude and skewness induced errors. Finally, we investigated the possibility of applying empirical corrections to the Geosat data and established a minimum averaging time in order that the estimated corrections remain stable. This algorithm is currently being used to reprocess Topex data and the results will be discussed in a separate paper.

Appendix A

In this appendix, we derive expressions for the return waveform and its derivatives for the case when the point target response can be written as a series of Gaussians. The return waveform is the convolution of three terms [Brown, 1977]: the smooth surface response, the point target respouse, and the surface specular point probability density function. This last

quantity is given by

$$f_o(t) = \frac{1}{\sqrt{2\pi\sigma_o^2}} \exp\left[-\frac{(t-t_o)^2}{2\sigma_o^2}\right]\left[1 - \frac{\lambda}{6}\left(\frac{(t-t_o)^3}{\sigma_o} - 3\frac{(t-t_o)}{\sigma_o}\right)\right] \tag{12}$$

where, rather than expressing the pdf in the height domain (2), we have expressed it in the delay time domain ($t = -2z/c$), where c is the speed of light. In the previous equation, t_o represents the mean level of the specular points on the ocean surface, and σ_o represents the standard deviation, in delay time units, of the specular points about this mean. It is well known that the mean electromagnetic surface need not coincide with the mean Sea surface, giving rise to the "Electromagnetic Bias" [Rodríguez,1988]. On the other hand, if geometric optics is correct, the deviation of the higher order cumulants from the sea surface cumulants is believed to be of second order, or higher, in the wave slope, and hence can be ignored [Rodríguez,1988].

The smooth surface response is given by [Rodríguez,1988]

$$S(t) = U(t)\exp[-\alpha t]\, I_0(\beta\sqrt{t}) \tag{13}$$

$$\alpha = \ln 4 \frac{c}{h(1+h/R)} \frac{\cos\xi}{\sin^2\theta_0^2} \tag{14}$$

$$\beta = \ln 4 \sqrt{\frac{c}{h(1+h/R)}} \frac{\sin 2\xi}{\sin^2\theta_0^2} \tag{15}$$

where $U(t)$ represents the unit step function, I_0 is the zeroth order Bessel function of the first kind, h is the altimeter height above the surface, R is the radius of the earth, ξ is the off-nadir angle, and θ_0 is the antenna beamwidth half-cone angle.

Using the fact that convolution is a linear operator, it is sufficient to obtain the result of the convolution using a Gaussian of arbitrary amplitude c_i, displacement, t_i, and standard deviation, s,. The final result follows by linear superposition. In the presence of skewness, the ocean specular point distribution convolved with a Gaussian function can be written as

$$f_o \otimes c_i \exp\left[-\frac{(t-t_i)^2}{2\sigma_i^2}\right] = c_i\frac{\sigma_i}{\sigma}\exp\left[-\frac{(\tau^2}{2\sigma^2}\right]\left[1 - \left(\frac{\sigma_o}{\sigma_i}\right)^3 \frac{\lambda}{6}\left(\tau^3 - 3\tau\right)\right] \tag{16}$$

$$\tau = \frac{t - t_o - t_i}{\sigma} \tag{17}$$

$$\sigma = \sqrt{\sigma_i^2 + \sigma_o^2} \tag{18}$$

The convolution of equation (16) with the smooth surface responses cannot be performed analytically. however, if the off-nadir angle is of the same order of magnitude, or smaller, than half the antenna beamwidth, one can approximate the Bessel function above as

$$I_0(z) \approx 1 + \frac{z^2}{4} + \frac{z^4}{64} \tag{19}$$

This approximation is better than 2% for $z < 2$. The convolution can now be carried out in a straightforward, if tedious, fashion. The result, correct to the same order of approximation, is

$$p_i(\tau) = K(\tau)[C_1(\tau) + C_2(\tau)] + L(\tau)\frac{1}{\sqrt{2\pi}}\exp\left[-\frac{\tau^2}{2}\right](1 - C_3(\tau)) \tag{20}$$

$$K(\tau) = A\sqrt{2\pi\sigma_i^2}\exp(-d\tau)I_0\left(\zeta\sqrt{d\tau}\right) \tag{21}$$

$$C_1(\tau) = \frac{1}{2}\left[\operatorname{erf}\left(\frac{\tau}{\sqrt{2}}\right) + 1\right] \tag{22}$$

$$C_2(\tau) = \left(\frac{\sigma_o}{\sigma_i}\right)^3 \frac{\lambda}{6}\frac{1}{\sqrt{2\pi}}\exp\left[-\frac{\tau^2}{2}\right](\tau^2 + 3d\tau - 1) \tag{23}$$

$$L(\tau) = A\sqrt{2\pi\sigma_i^2}\exp(-d\tau)\frac{\zeta^2 d}{4} \tag{24}$$

$$C_3(\tau) = \left(\frac{\sigma_o}{\sigma_i}\right)^3 \frac{\lambda}{6}\left(\tau^3 + 3d\tau^2 + 3d\right) \tag{25}$$

$$d = \alpha\sigma \tag{26}$$

$$\zeta = \frac{\beta}{\sqrt{\alpha}} \tag{27}$$

$$\tau = \frac{t' - t_o - t_i}{\sigma} \cdot d \tag{28}$$

Notice that, when $\tau >> 0$, the return power asymptotically approaches the smooth surface response. This asymptotic behavior of the power can be shown to be a general property of the return waveform for point target responses and surface pdf's which go to zero asymptotically at a fast enough rate.

Using the previous results, the final expression for the mean return power is given by

$$p(\tau) = \sum_i c_i p_i(\tau) \tag{29}$$

Having expressed the return power as a sum of analytic functions, the derivatives of the power can be explicitly calculated by computing the derivatives of each term in the sum and adding them. These derivatives are given by the following formulas

$$\frac{\partial p_i}{\partial A} = \frac{p_i}{A} \tag{30}$$

$$\frac{\partial p_i}{\partial \zeta^2} = \frac{p_0}{2}\sqrt{\frac{d\tau}{\zeta^2}}\frac{I_1(\zeta\sqrt{d\tau})}{I_0(\zeta\sqrt{d\tau})} + \frac{p_1}{\zeta^2} \tag{31}$$

$$\frac{\partial p_i}{\partial t_o} = \frac{\mathrm{d}}{\sigma}p_i - \frac{1}{\sqrt{2\pi\sigma^2}}\exp\left[-\frac{\tau^2}{2}\right]\left\{K(\tau) - 7//(,))\left[1 - \left(\frac{\sigma_o}{\sigma_i}\right)^3\frac{\lambda}{6}\left(\tau^3 + 3d\tau^2 - 3\tau\right)\right]\right.$$
$$- \frac{p_0\zeta}{2\sigma}\sqrt{\frac{d}{\tau}}\frac{I_1(\zeta\sqrt{d\tau})}{I_0(\zeta\sqrt{d\tau})} + \frac{p_1}{\zeta^2} \tag{32}$$

$$\frac{\partial p_i}{\partial \sigma_o} = -\frac{\sigma_o}{\sigma}\frac{1}{\sqrt{2\pi\sigma^2}}\exp\left[-\frac{\tau^2}{2}\right]\left(-\tau K(\tau) + \tau^2 L\right) + \left(\frac{\sigma_o}{\sigma_i}\right)^3\frac{\lambda}{6}$$
$$\left[\tau K(\tau)\left(\tau^3 + 3d\tau^2 - 3\tau + 3d\right) - L(\tau)\left(\tau^5 + 3d\tau^4 - 3\tau^3 + 3d\tau^2 + 6d\right)\right]\Big]$$
$$+3\frac{K(\tau)}{\sigma_o}C_2 + 3\frac{L(\tau)}{\sigma_o}\frac{1}{\sqrt{2\pi}}\exp\left[-\frac{\tau^2}{2}\right]C_3 \tag{33}$$

$$\frac{\partial p_i}{\partial \lambda} = K(\tau)\frac{C_2}{\lambda} - L(\tau)\frac{1}{\sqrt{2\pi}}\exp\left[-\frac{\tau^2}{2}\right]\frac{C_3}{\lambda} \tag{34}$$

$$p_0 = K(\tau)(C_1(\tau) + C_2(\tau)) \tag{35}$$

$$p_1 = L(\tau)\frac{1}{\sqrt{2\pi}}\exp\left[-\frac{\tau^2}{2}\right](1 - C_3(\tau)) \tag{36}$$

The reader will notice that we have computed the partial derivative of the power with respect to ζ^2 rather than ζ. This subtlety is due to the fact that, as $\zeta \to 0$, then $\frac{\partial p_i}{\partial \zeta} \to 0$, which implies that, close to vanishing attitude (the nominal condition!), the power becomes completely insensitive to attitude, and hence the attitude cannot be estimated, However, the return power is not insensitive to attitude squared, even for vanishing attitudes. The price one pays for being able to estimate this parameter is that, due to the presence of noise, a negative value of attitude squared will sometimes be estimated: the asymptotic distribution of the estimates of the attitude squared when the true attitude is zero is a Gaussian centered at zero attitude squared, and in this case half of the values estimated will be negative. This inconvenience may be ameliorated by averaging the estimates (which

will asymptotically produce an unbiased estimator) or by setting all negative values to zero (which will produce a biased estimate).

The equations for the partial derivatives are somewhat complicated, but they simplify significantly if the derivatives are taken about $\lambda = 0$, as has, in fact, been done in the implementation of the algorithm. The partial derivative of the total power with respect to any variable x can now be written as

$$\frac{\partial p}{\partial x} = \sum_i c_i \frac{\partial p_i}{\partial x} \tag{37}$$

which is the relationship needed for implementing our algorithm.

Acknowledgement

The research described in this paper was carried out by the Jet Propulsion Laboratory, California Institute of Technology, under contract with the National Aeronautics and Space Administration.

References

Berger, T., "Satellite altimetry using ocean backscatter," IEEE Trans. Antennas Propag., AP-20(3), 295-309, 1972.

Brenner, A. C., C.J. Koblinsky, and H.J. Zwally, "Postprocessing of satellite altimetry return signals for improved sea-surface topography accuracy, J. Geophys. Res., 98, C1, 933-944, 1993.

Brown, G.S., "The average impulse response of a rough surface and its applications," IEEE 'i'rails. Antennas Propag., A P-2,5(1), 67-74, 1977.

Chelton, D., Walsh, E. J., MacArthur, J.],., "Pulse compression and sea level tracking in satellite altimetry," J. Atmos. and Oceanic Tech., Vol. 6, no. 3, 407-437, 1989.

"Geosat-A data users/ground system ICD," JHU/APL document 792-9510, The Johns Hopkins University, Applied Physics Laboratory, Laurel, MD 20707, 1985.

Goodman, J. W., "Statistical Optics, " Wiley-Interscience, New York, 1985.

Gradshteyn, 1. S., and I.M. Ryzhik. Table of Integrals, Series, and Products, Academic 1'1'('ss, 1980.

Hayne, G. S., and D. W. Hancok. "Corrections for the effects of significant wave height and attitude on Geosat radar altimeter measurements," J. Geophys. Res., 95, C3, 2s37-2s.12. 1990.

Lipa, B. J., and D.E. Barrick, "Ocean surface height-slope probability density function from Seasat altimeter echo," J. Geophys. Res., 86 (C11), 10,921-10,930, 1981.

Rodriguez, E., "Altimetry for non-Gaussian oceans: height biases and estimation of parameters," J. Geophys. Res., 93, C11, 14, 107-14,120, 1988.

Sorenson, H.W., "Parameter Estimation," Marcel Dekker, Inc., New York, 1980.

Srokosz, M. A., and M. Longuet-Higgins, "On the skewness of sea surface elevation ," J, Fluid Mech., 164, -1 S7--197, 1986.

Srokosz, M ..4., and P. G. (hallenor, "The use of maximum likelihood estimation to derive geophysical parameters from radar altimeter data," Chelton, D.B. (cd.), WOCE/NASA Altimeter Algorithm Workshop, Technical Report No. 2, Appendix, U.S. Planning Office for WOCE, College Station, TX, 1988.

Tsang, L., J ..4. Kong, and R.T. Shin, Theory of Microwave Remote Sensing, Wiley-Interscience, 1985

Walsh, E.J., "Pulse-to-pulse correlation in satellite radar altimeters", Radio Science, 17 (4), 786-800, 1982.

Zieger, A.R., D.W. Hancock, G. S. Hayne, and C.L. Purdy, "NASA radar altimeter for the Topex Poseidon project," Proc. IEEE, 79(G), 810-826, 1991.

Figure Captions

Figure 1 :A comparison of the exact theoretical point target response and the one obtained by the Gaussian pseudo-wavelet decomposition (solid curves). The dashed curve shows the difference between the two curves.

Figure 2: Monte Carlo performance of the estimation algorithm. a) Height estimation performance: the squares show the Topex instrument pre-launch performance for one second data averaging; the solid circles show the maximum likelihood performance. These estimates are uncorrelated from sample to sample, unlike the altimeter tracker estimates, which are correlated due to the on-board tracking (smoothing) algorithm. The lowest curve shows the algorithm performance with the same amount of smoothing as the Topex on-board tracker. b) Significant wave height performance (same symbols as in (a)), c) Skewness estimation performance.

Figure 3: Fractional residuals from the waveform fit (a) and from a waveform computed using the parameters in the GDR's. The dashed curves show the residuals using the calibration point target response which show large errors for both the retracked and the GDR estimated parameters. The solid line shows the residuals after PTR optimization. Notice that even after PTR optimization, the GDR estimates show large residuals about the leading edge. This is consistent with the height errors shown in the following figures. Notice also that the GDR residuals show a trend in the trailing edge: this inconsistent with tile attitude errors discussed in the text.

Figure 4: Comparison of the calibration PTR (dashed line) and the optimized PTR (solid line). Notice that the differences are small, but, as shown in the previous figure, can have significant effects on the residuals,

Figure 5: Measured height noise for weighted (a) and unweighed (b) estimation, The points show the measurements, while the solid lines are the Monte Carlo predictions. A good agreement is observed between theory and observation. The weighted algorithm performs somewhat better for higher values of SWH, but the difference is not as marked for the smaller values of SWH.

Figure 6: A comparison of the waveform retracking estimated parameters and those

appearing in the GDR. The upper plot presents the percentage of the data in each bin, while the lower plot shows a binned scatter plot of the two quantities. The error bars represent the data variance in each bin. 6a) Significant Wave Height; 6b) Attitude squared; 6c) Height correction.

Figure 7: A histogram of the observed skewness for days 60-73 of 1988.

Figure 8: a) Retracking height correction binned as a function of SWH times attitude squared and SWH times skewness. b) Residuals from this surface after a best bit linear function is removed.

Figure 9: Retracking height collection binned as a function of SWH and attitude: a) average of data in days 60-66 of 1988; b) average of data in days 67-73 of 1988; c) average of data in the two week period. Notice that there is a significant amount of variation from week to week.

Figure 10: Residuals from tile previous surface after quadratic and cubic polynomials are removed. 10a) and lob) show the quadratic and cubic surfaces respectively. 10c) and 10d) show the corresponding residuals.

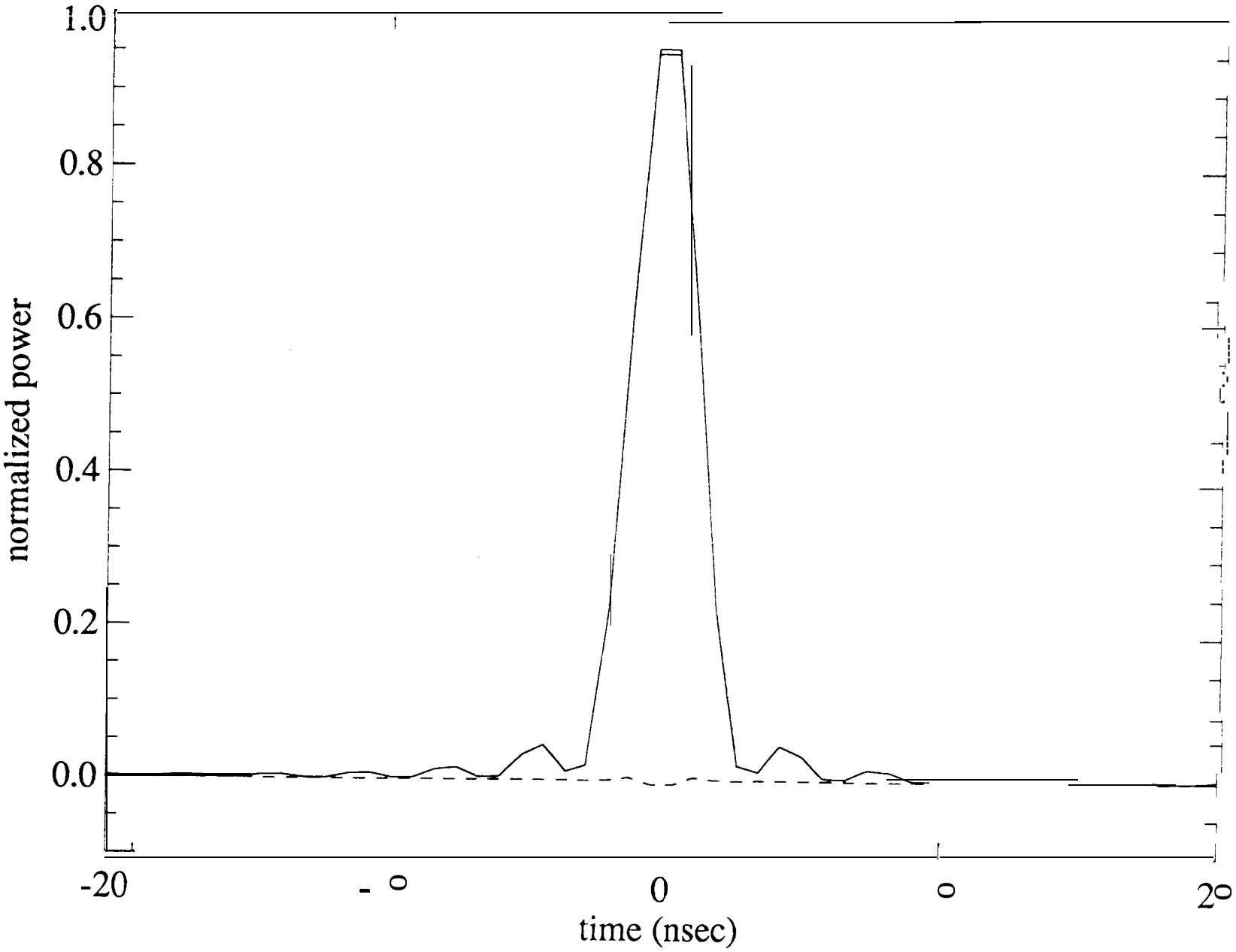

Figure 1

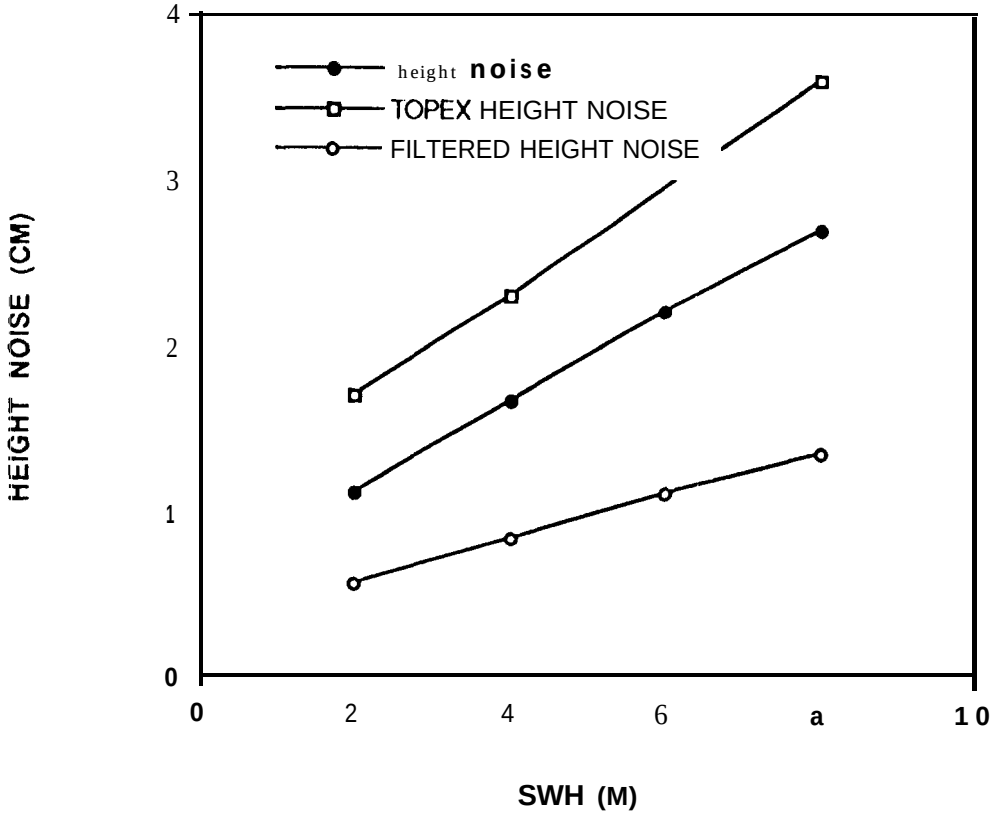
height noise
TOPEX HEIGHT NOISE
FILTERED HEIGHT NOISE
HEIGHT NOISE (CM)
SWH (M)
0
1
2
3
4
0
2
4
6
a
10

figure 2a

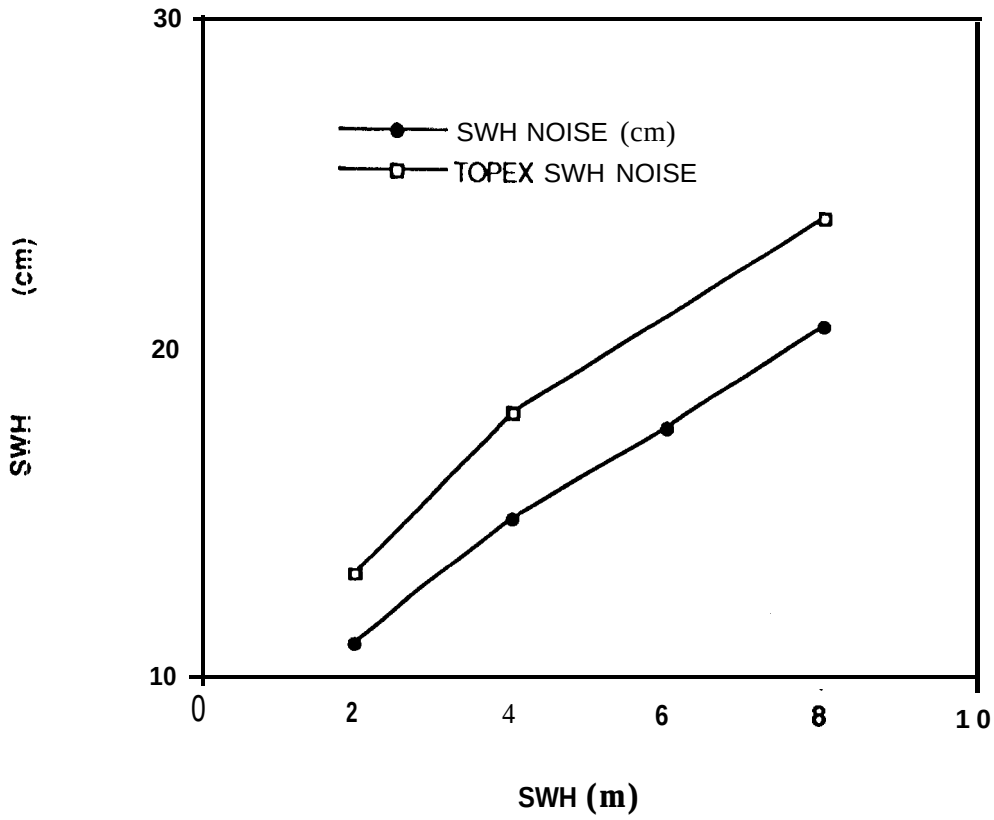

Figure 2b

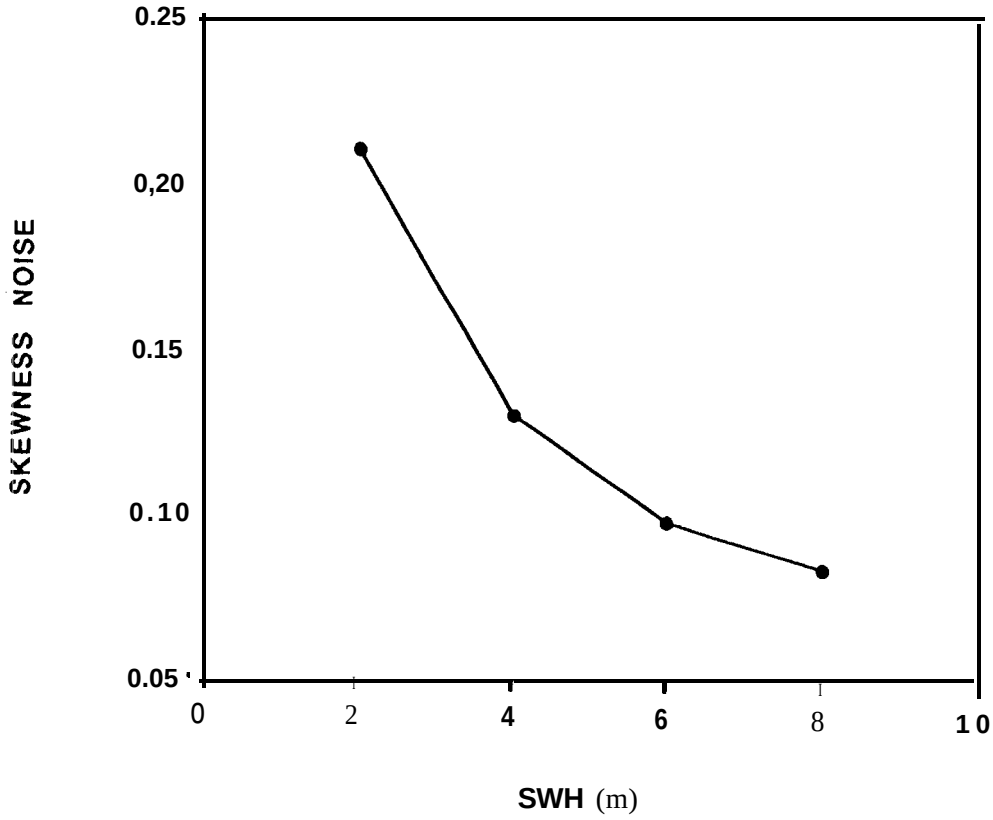

Figure 2c

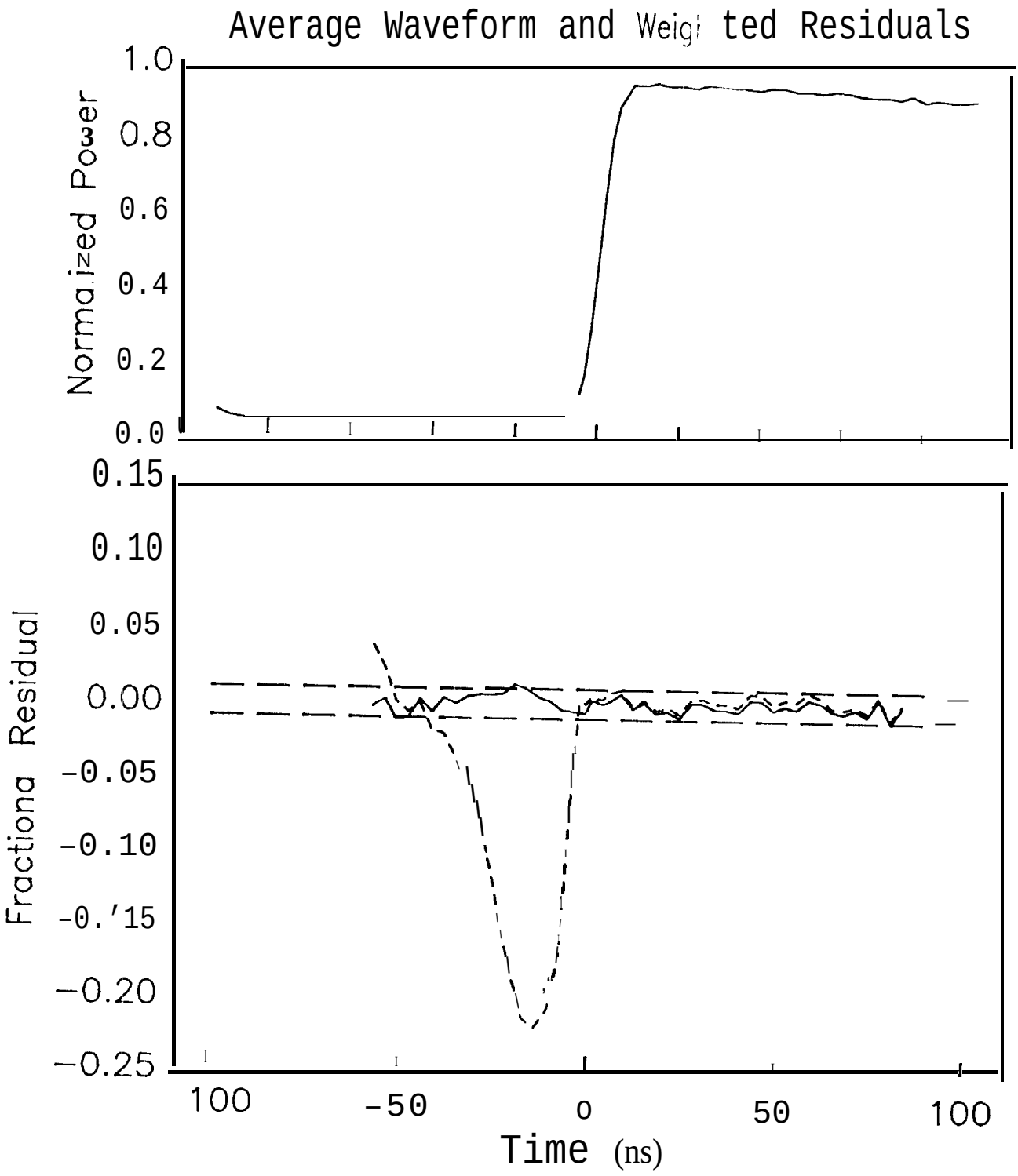
Average Waveform and Weighted Residuals
Normalized Power
1.0
0.8
0.6
0.4
0.2
0.0
Fractional Residual
0.15
0.10
0.05
0.00
-0.05
-0.10
-0.15
-0.20
-0.25
100
-50
0
50
100
Time (ns)

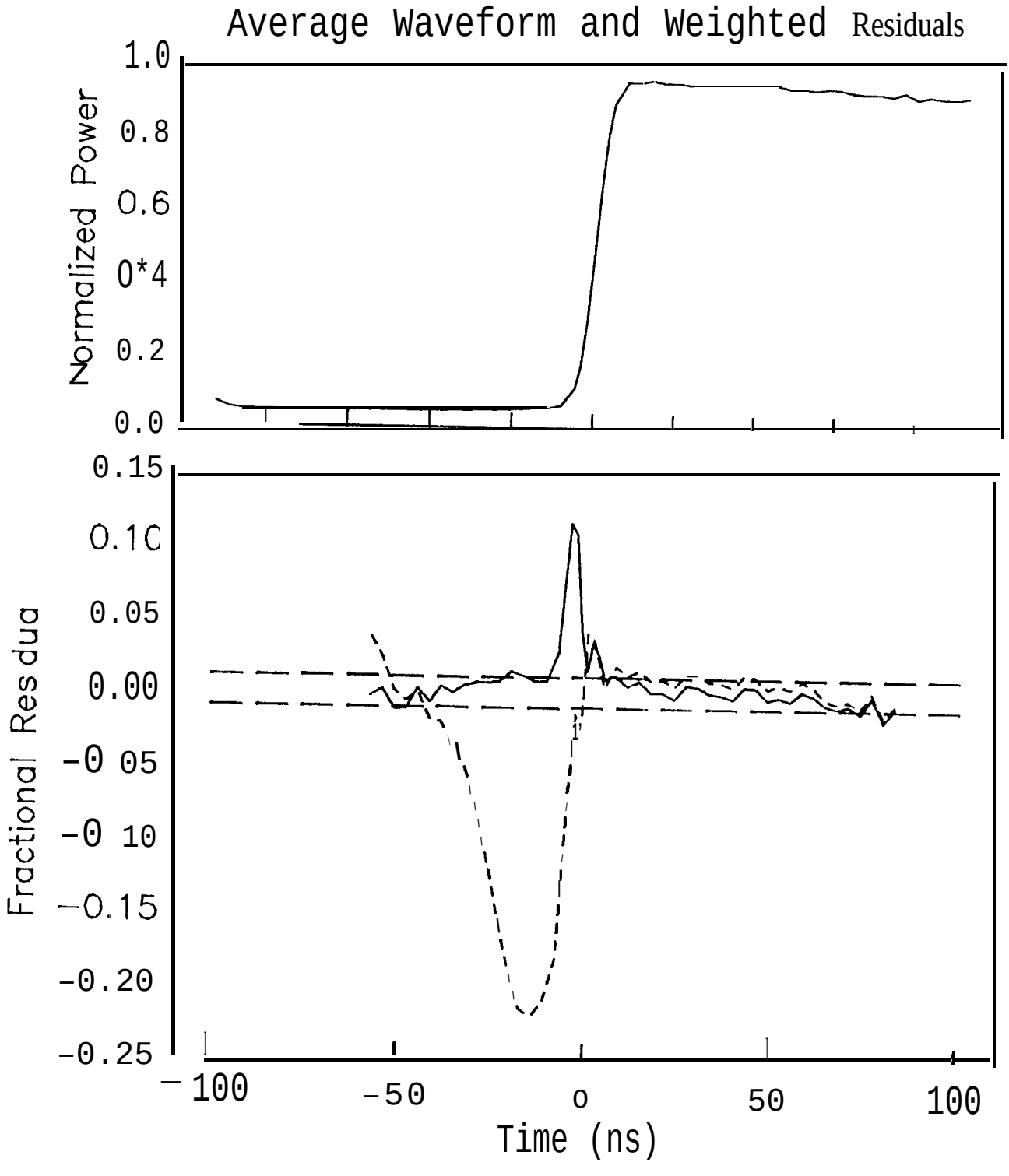
Average Waveform and Weighted Residuals
Normalized Power
1.0
0.8
0.6
0*4
0.2
0.0
Fractional Residua
0.15
0.10
0.05
0.00
-0 05
-0 10
-0.15
-0.20
-0.25
-100
-50
0
50
100
Time (ns)

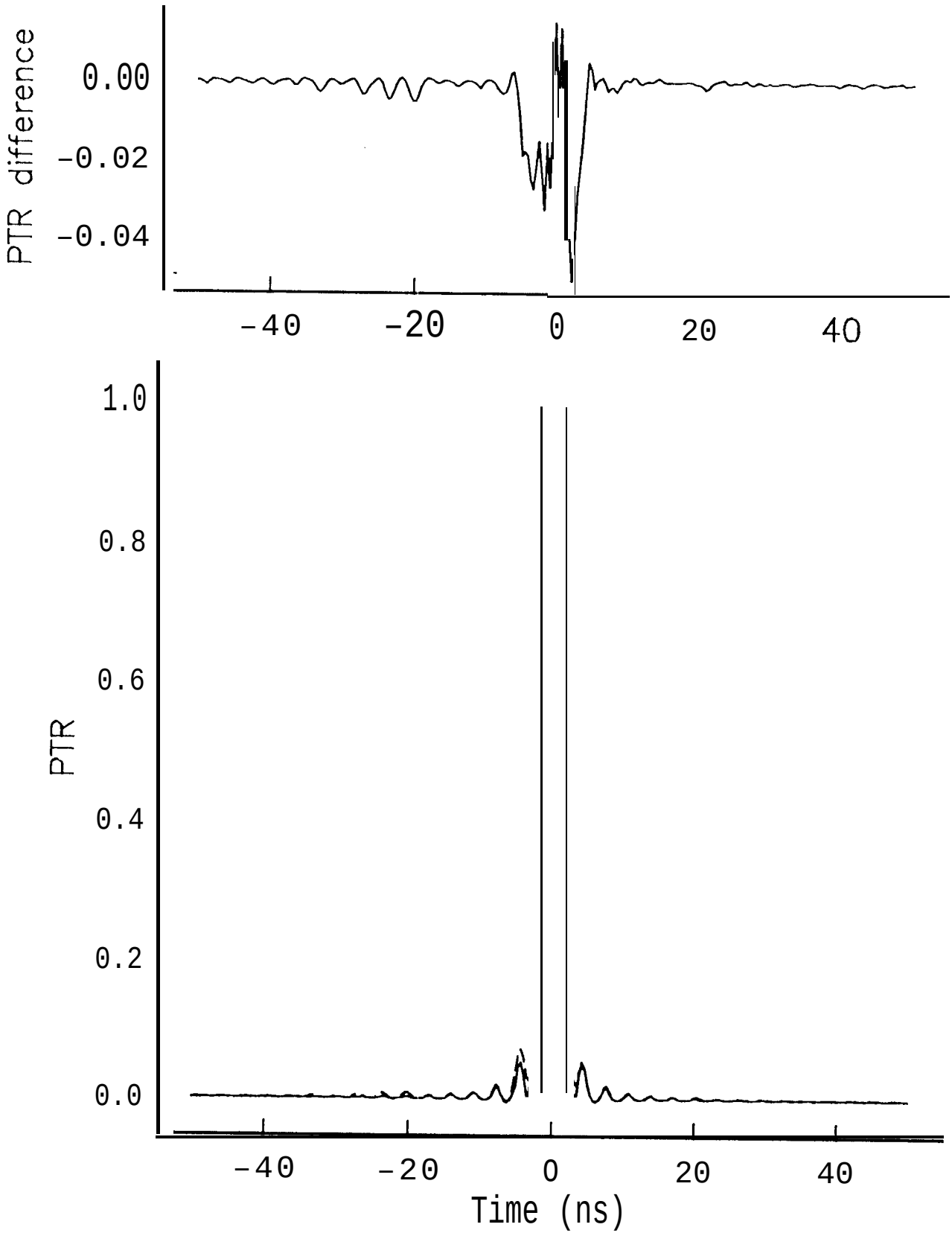
PTR difference
0.00
-0.02
-0.04
-40
-20
0
20
40
1.0
0.8
0.6
0.4
0.2
0.0
PTR
-40
-20
0
20
40
Time (ns)

Fig 5a

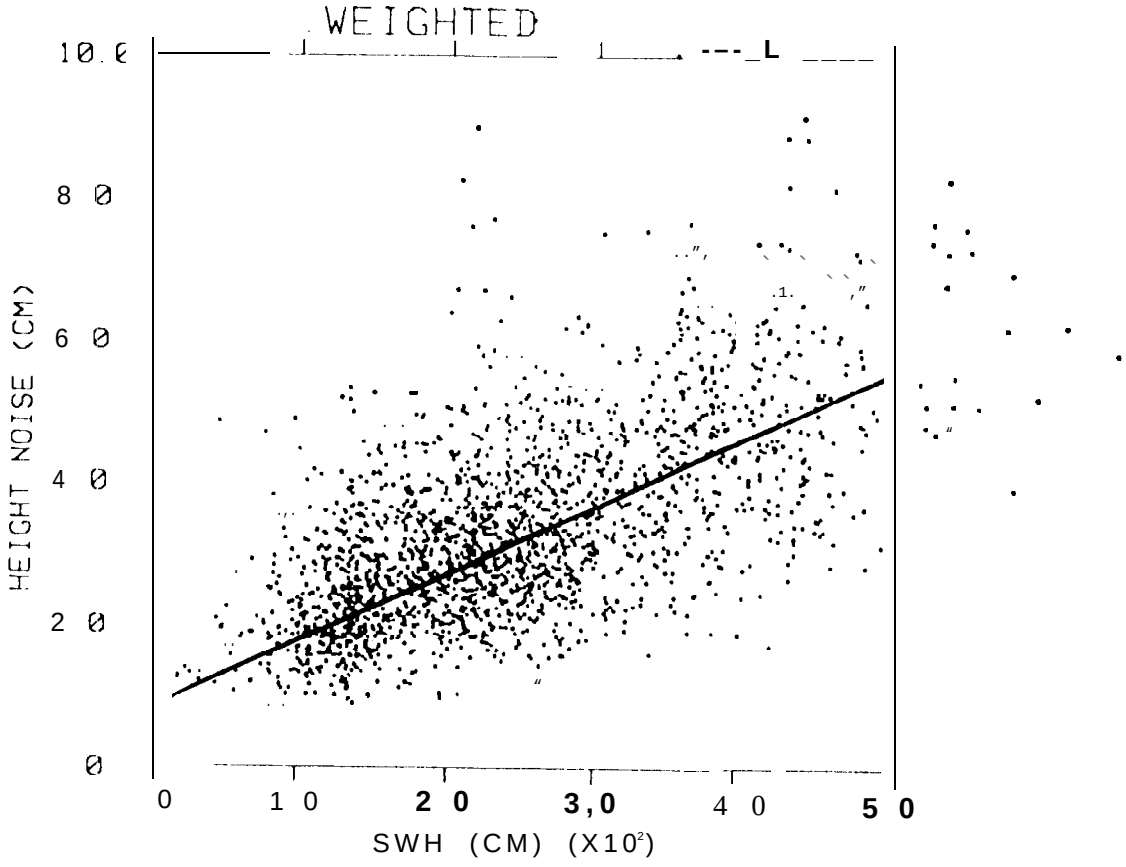
WEIGHTED
10.0
8 0
6 0
4 0
2 0
0
HEIGHT NOISE (CM)
0
1 0
2 0
3,0
4 0
5 0
SWH (CM) (X10²)

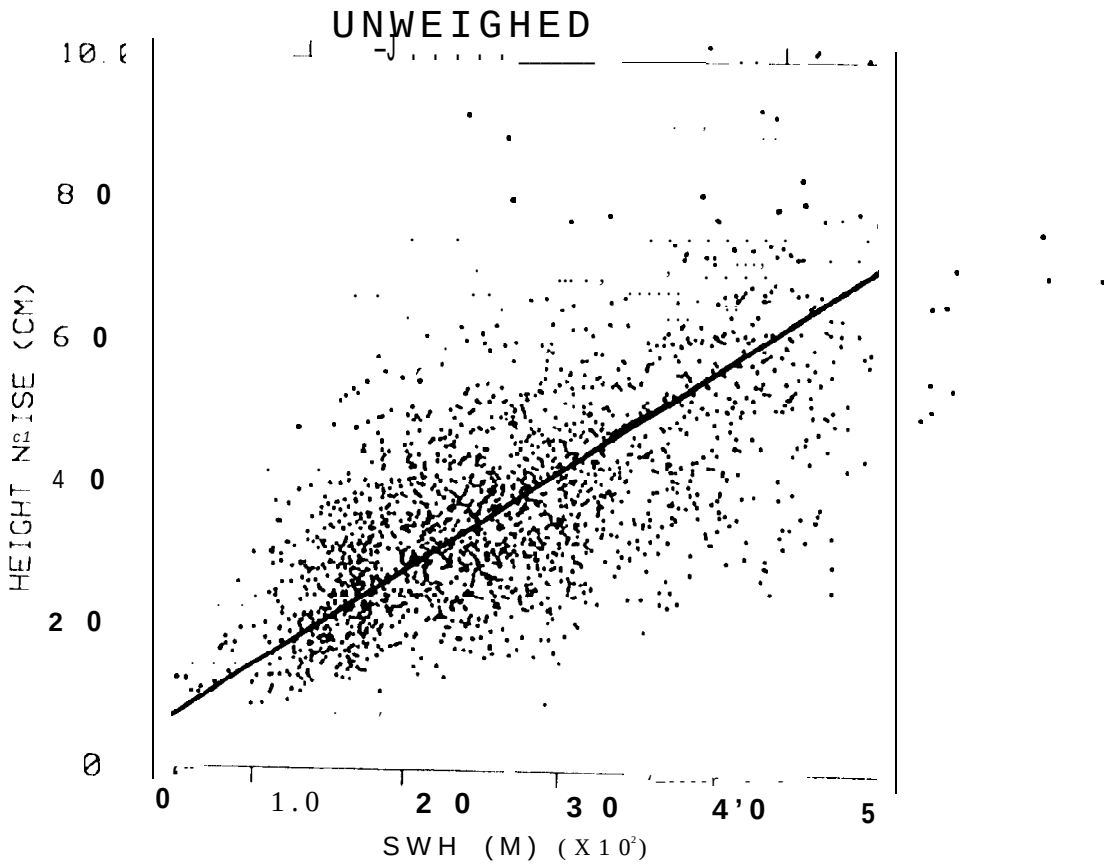
UNWEIGHED
10.0
8 0
6 0
4 0
2 0
0
HEIGHT NOISE (CM)
0
1.0
2 0
3 0
4'0
5
SWH (M) (X 10²)

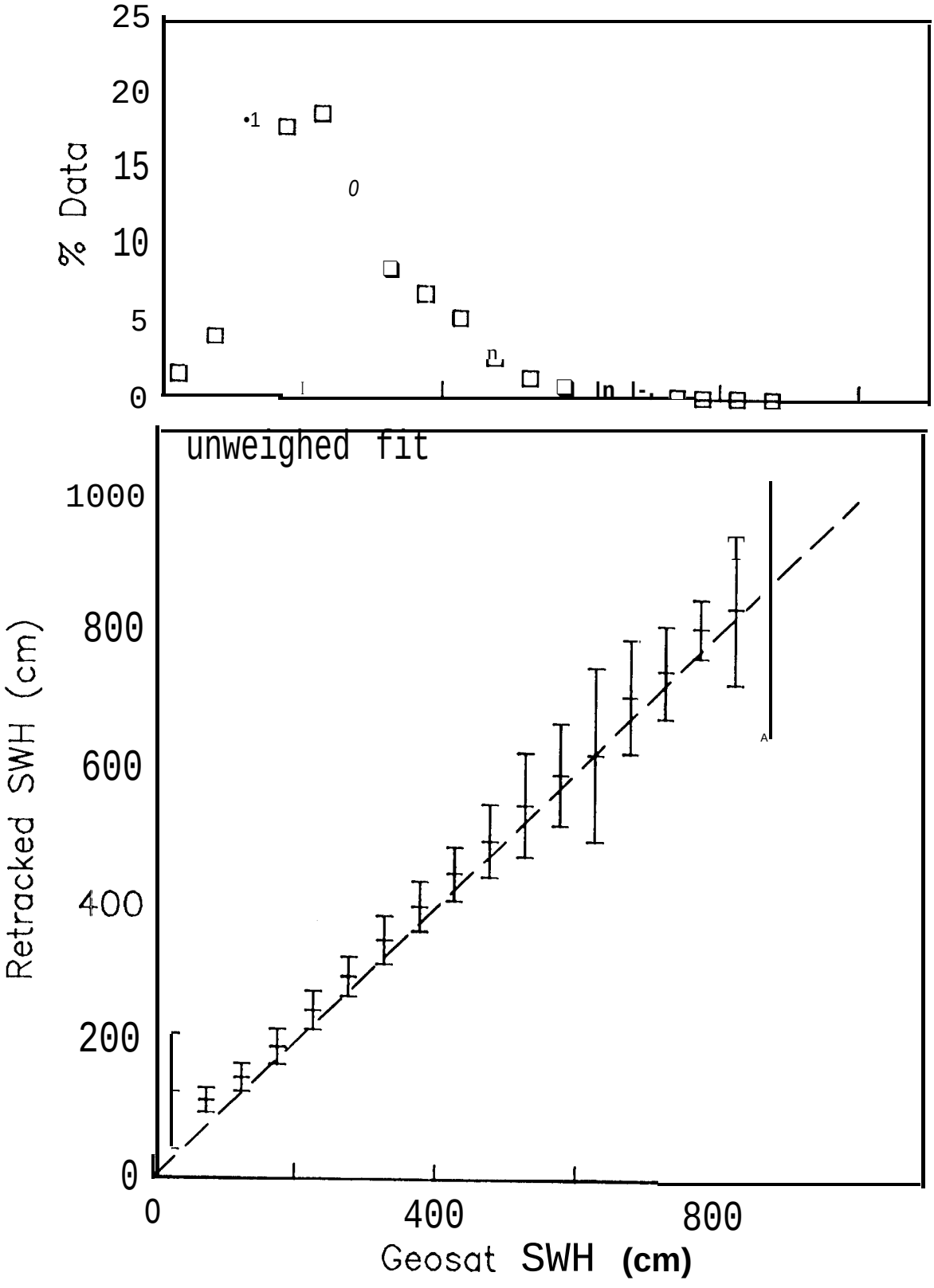
25
20
15
10
5
0
% Data
unweighed fit
1000
800
600
400
200
0
Retracked SWH (cm)
0
400
800
Geosat SWH (cm)

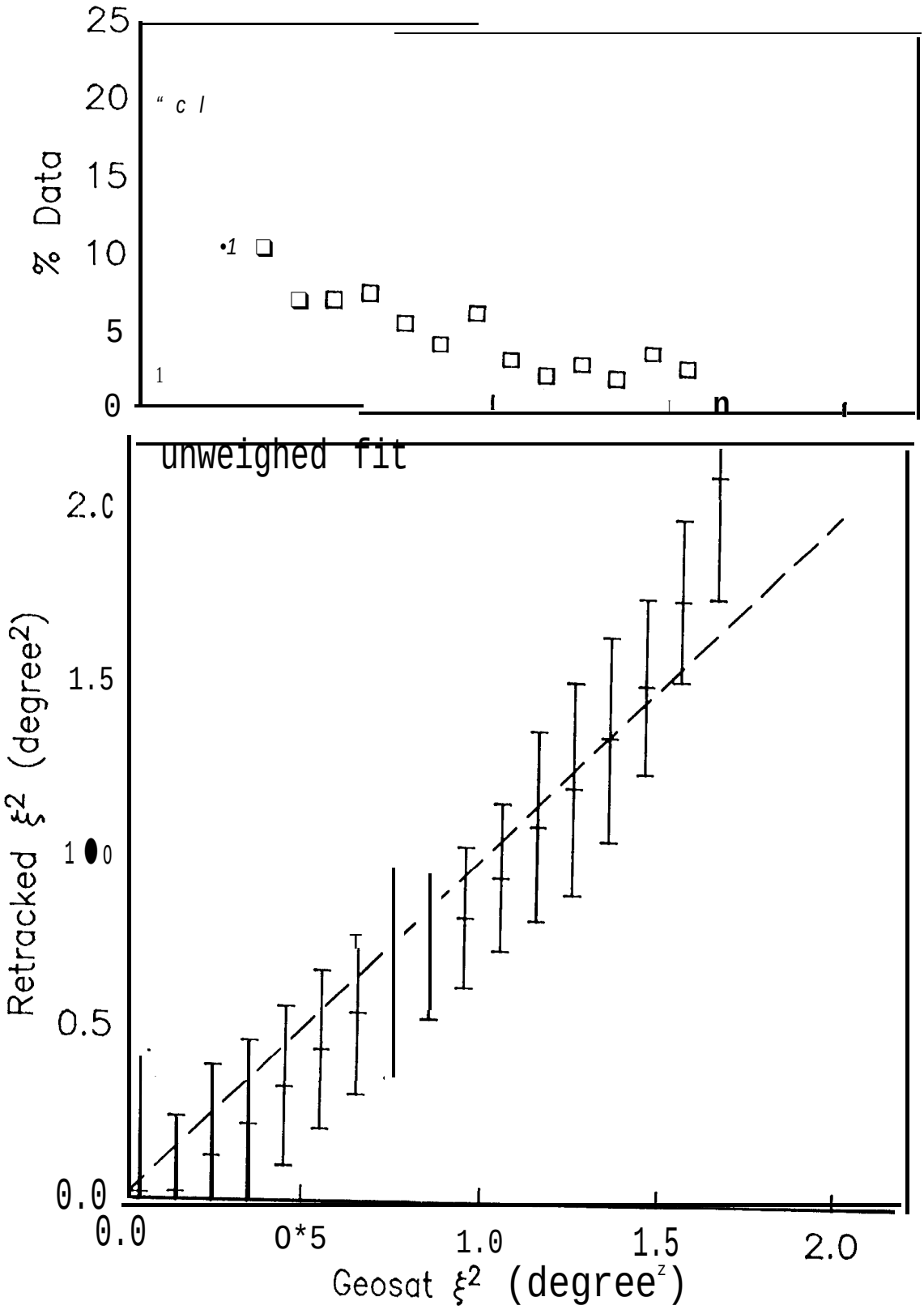
25
20
15
10
5
0
% Data
unweighed fit
2.0
1.5
1.0
0.5
0.0
Retracked ξ2 (degree2)
0.0
0*5
1.0
1.5
2.0
Geosat ξ2 (degree2)

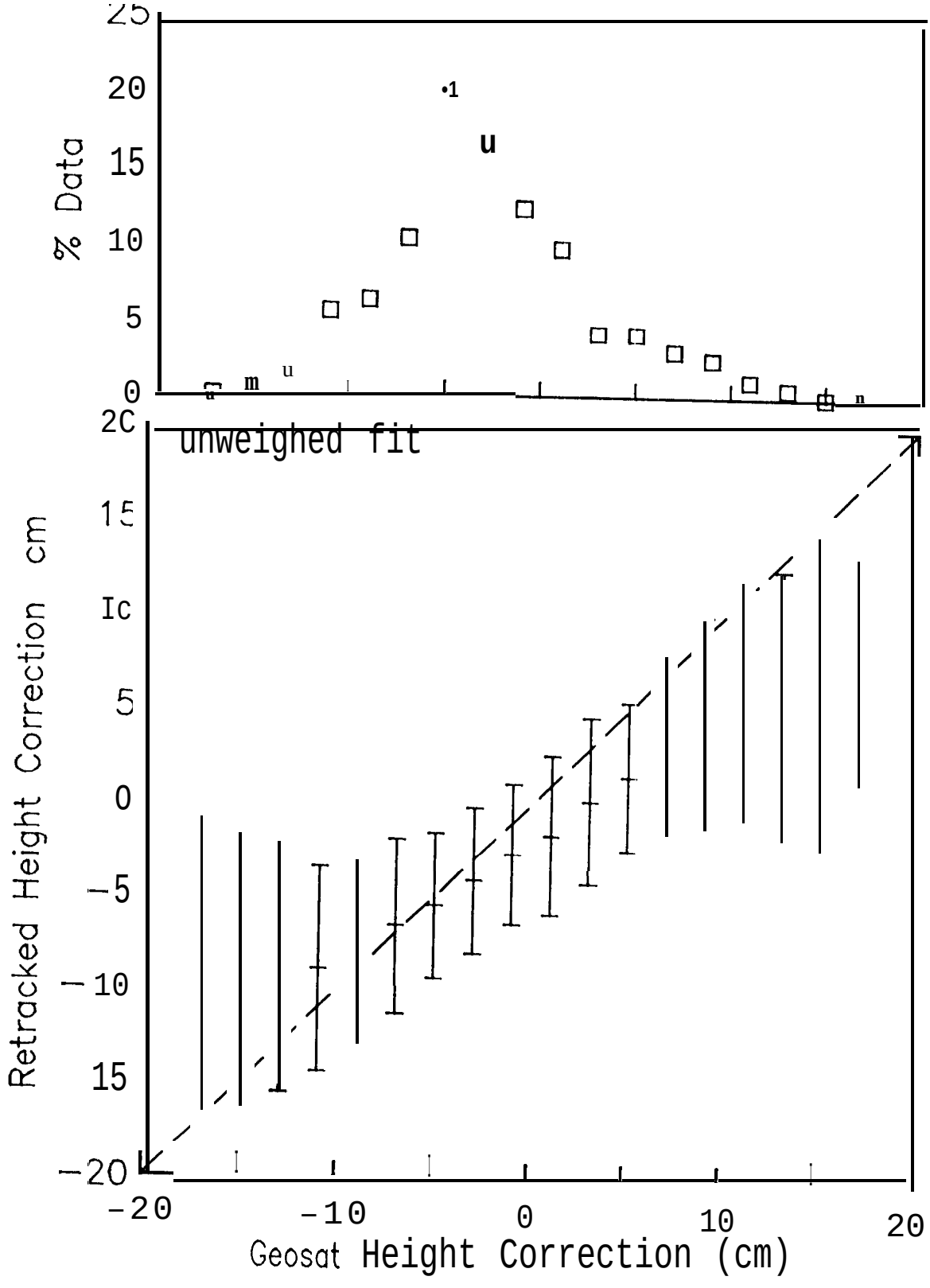
% Data
25
20
15
10
5
0
unweighed fit
Retracked Height Correction cm
20
15
10
5
0
-5
-10
-15
-20
-20
-10
0
10
20
Geosat Height Correction (cm)

Figure 7

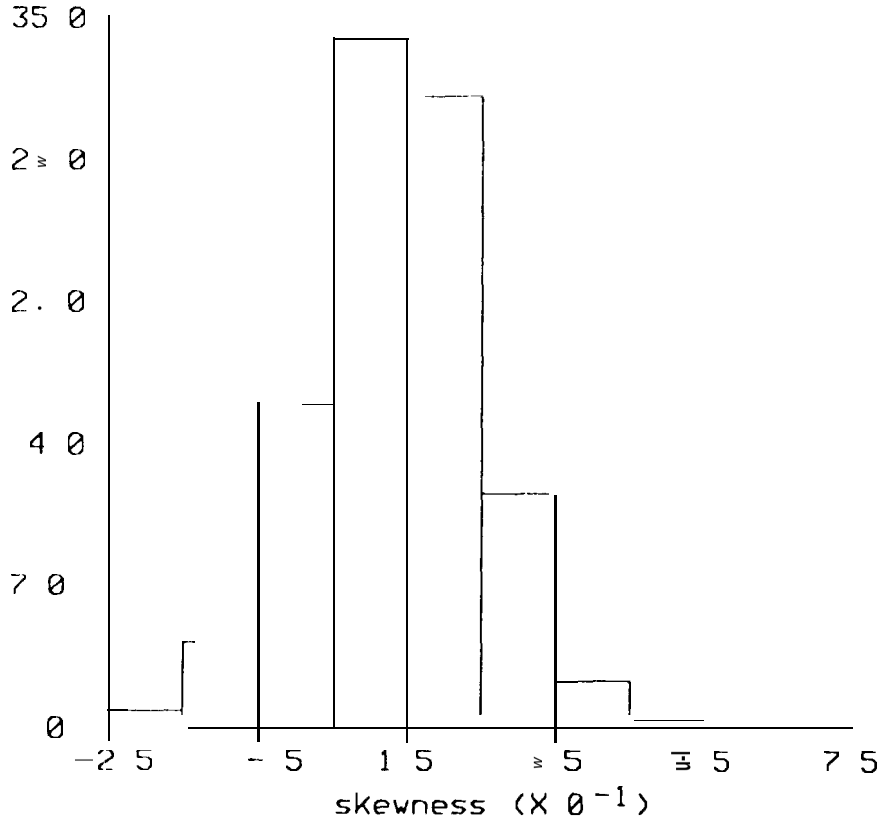

Figure 8a

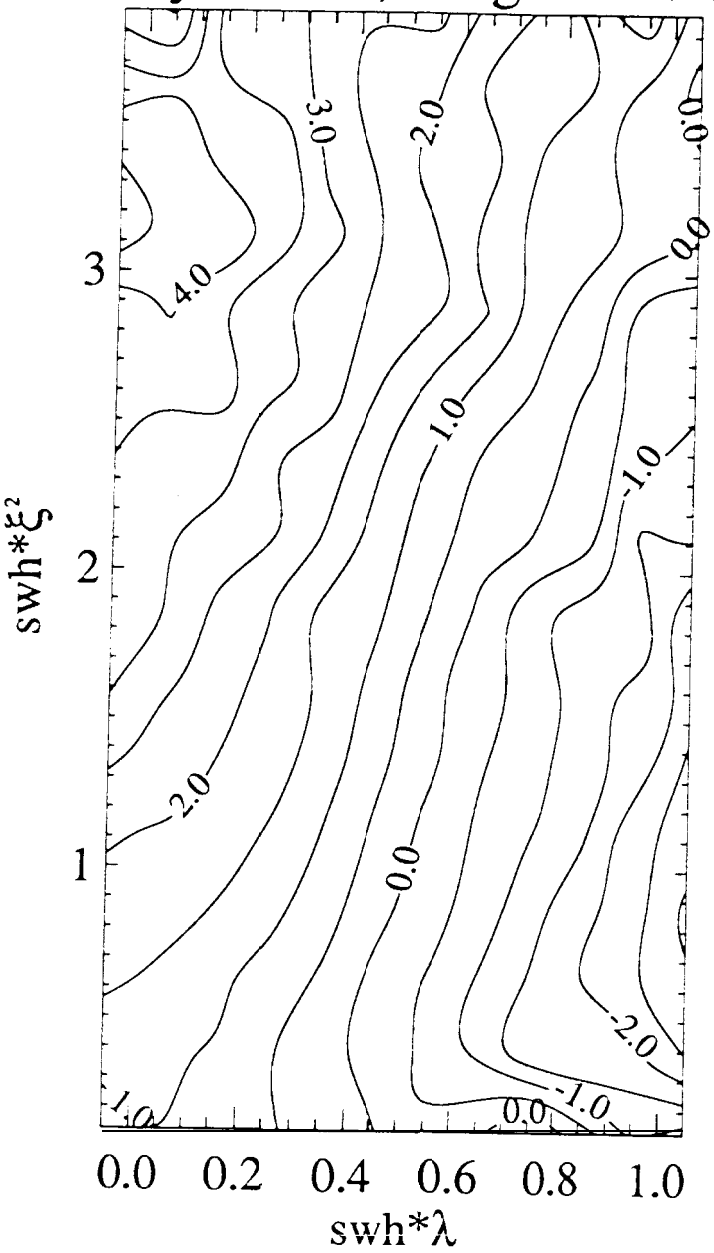

Figure 8b

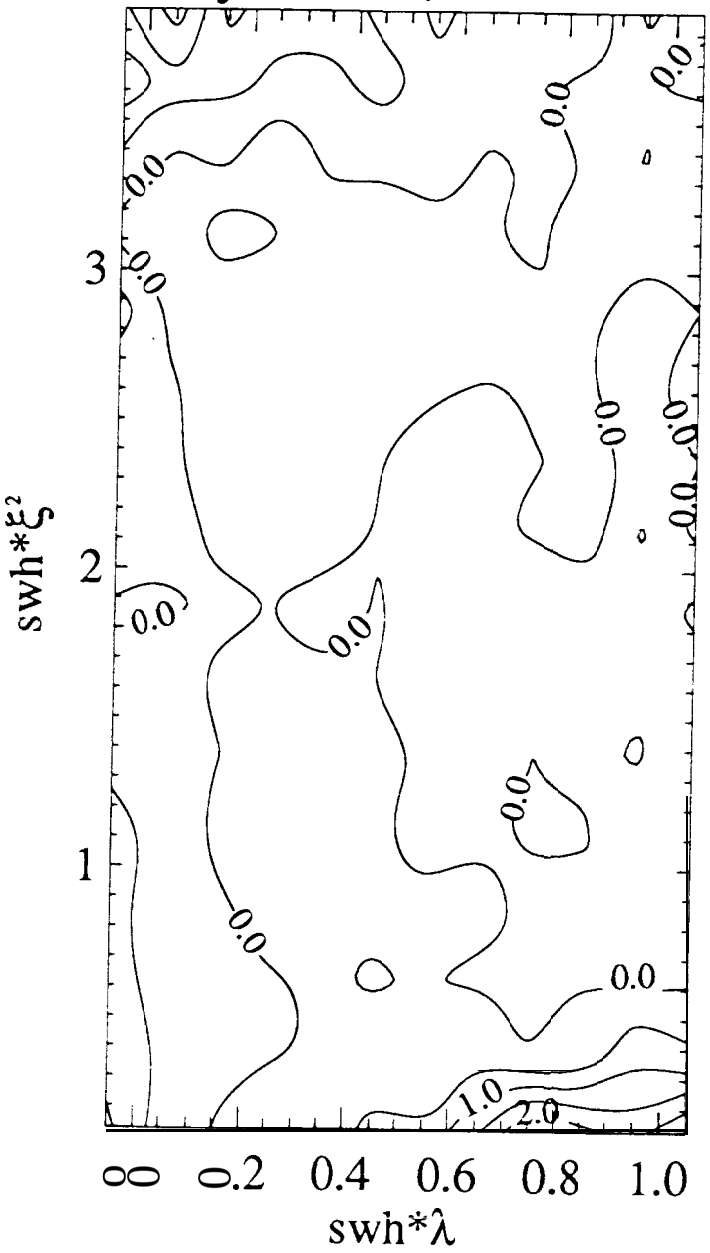

Fig 9b

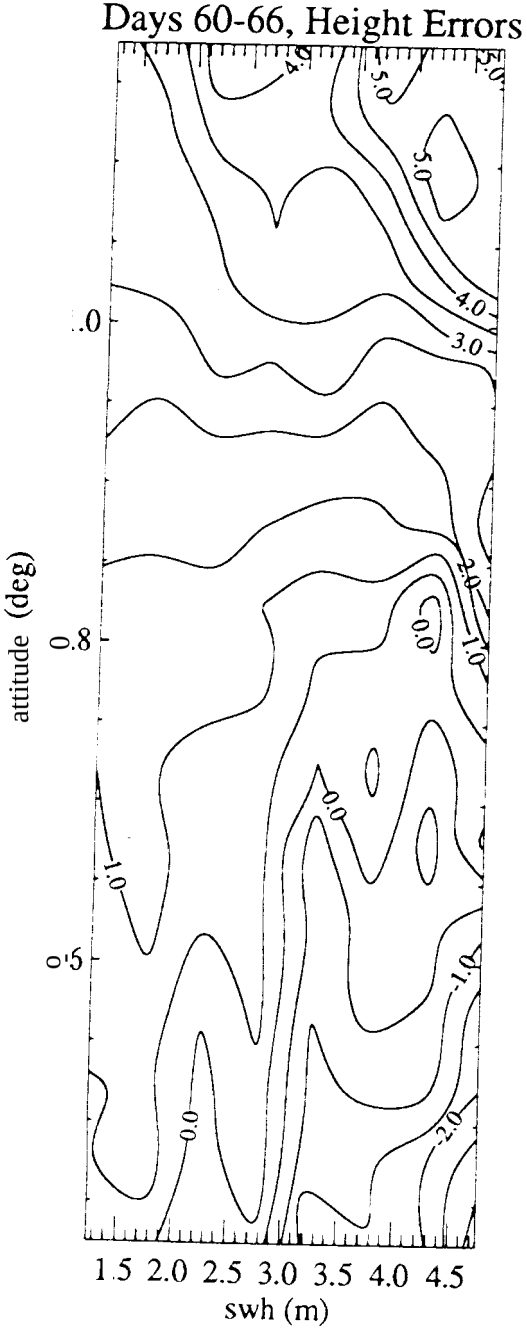
Days 60-66, Height Errors
attitude (deg)
swh (m)
1.5 2.0 2.5 3.0 3.5 4.0 4.5

Fig 9a

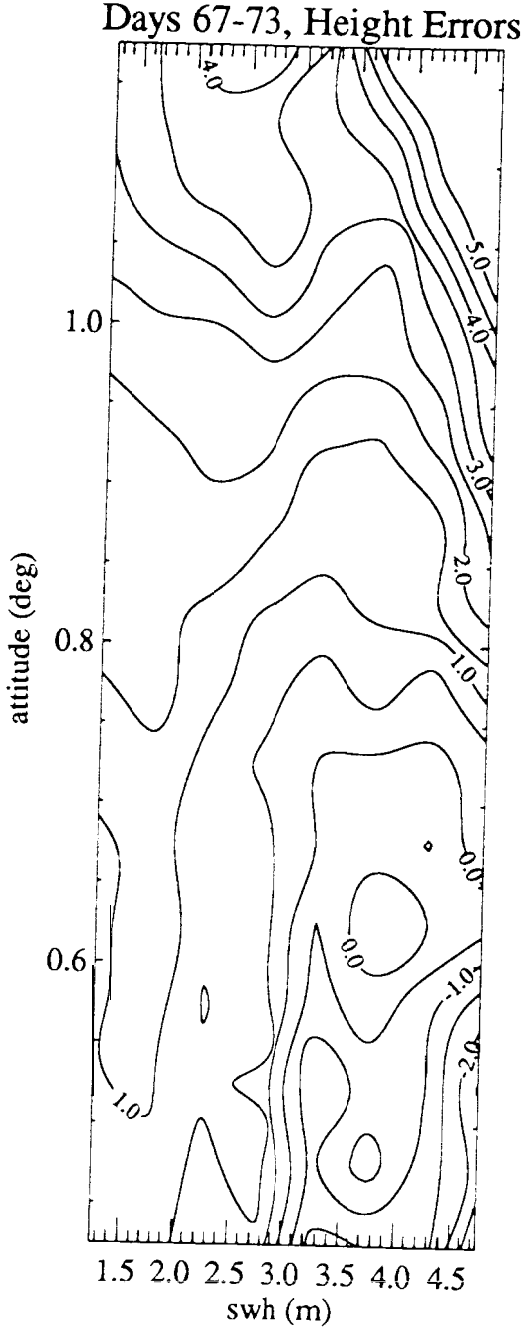
Days 67-73, Height Errors
attitude (deg)
1.0
0.8
0.6
swh (m)
1.5 2.0 2.5 3.0 3.5 4.0 4.5

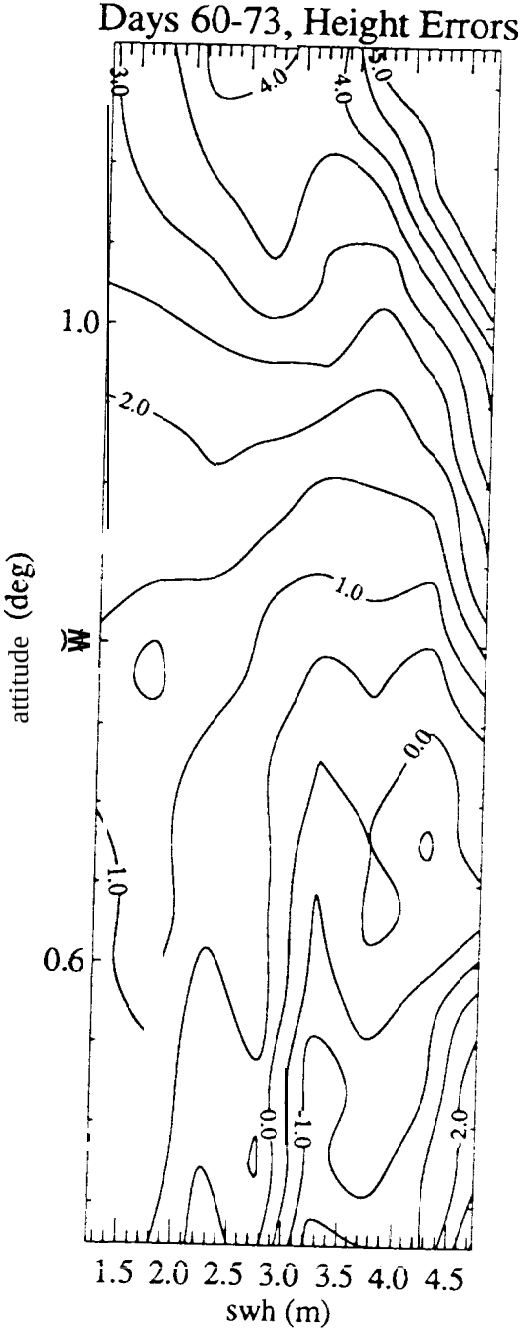
Days 60-73, Height Errors
attitude (deg)
1.0
0.6
swh (m)
1.5 2.0 2.5 3.0 3.5 4.0 4.5

Fig 10 b

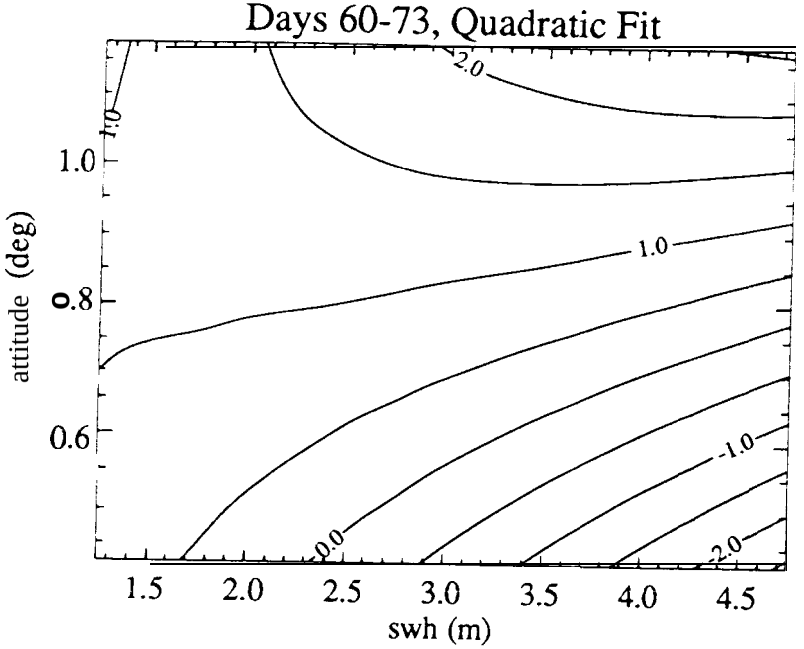

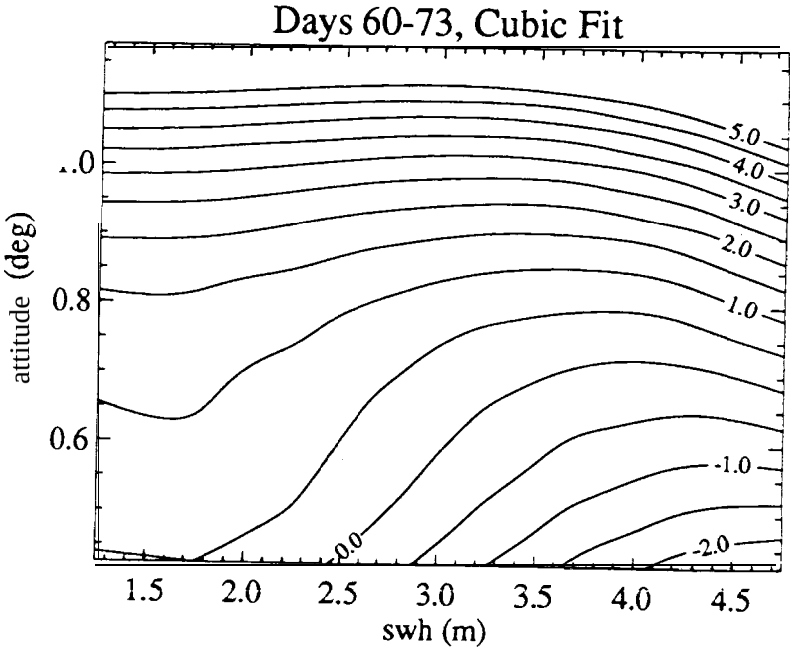

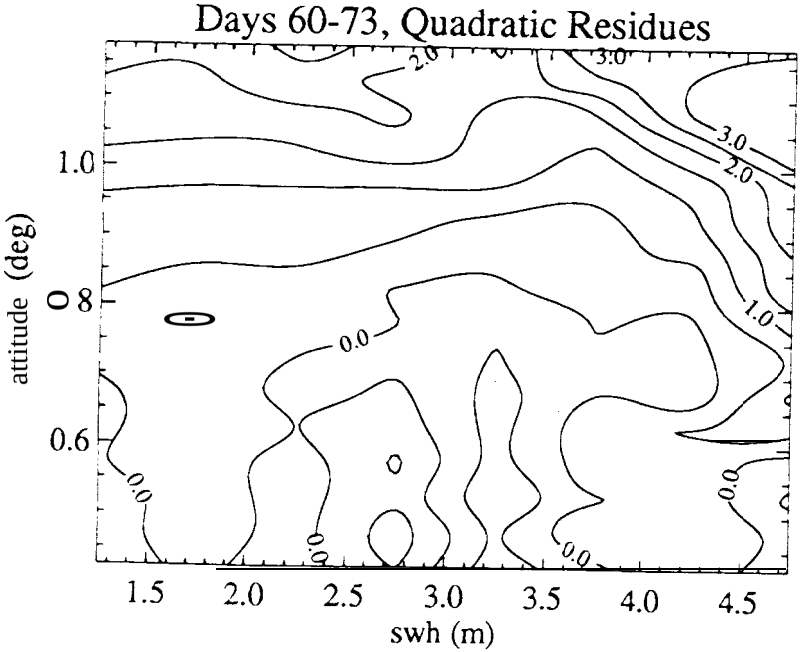

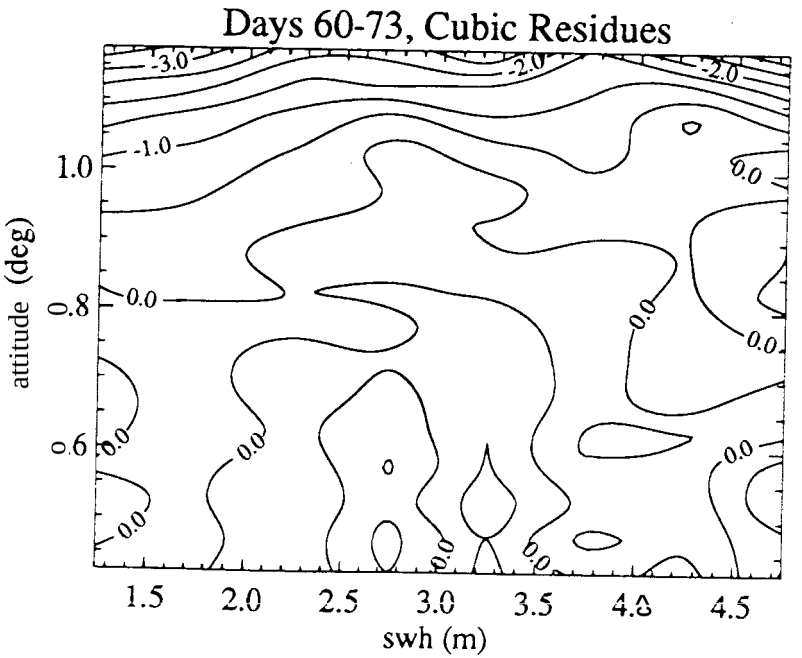

Fig 10 c

Fig 10 d